Role of Excited Core Rydberg States in Dissociative Recombination[†]

Steven L. Guberman*

Institute for Scientific Research, 22 Bonad Road, Winchester, Massachusetts 01890

Received: February 1, 2007; In Final Form: March 30, 2007

Intermediate states formed during the dissociative recombination of molecular ions with electrons can play significant roles in determining the magnitude of the total rate coefficient. These resonances are Rydberg states of two types, that is, they can have the ground or excited states of the ion as a core. Those with the excited cores have a fundamentally different excitation mechanism than those with the ground state core. The importance of excited core states in dissociative recombination has received only limited attention in the literature. Theoretical calculations on the dissociative recombination of N_2^+ are reported which compare the two types of resonances. Potential curves, electronic widths, cross sections, and rate coefficients are calculated for dissociative recombination along the $2^1\Sigma_g^+$ state, one of several routes for the dissociative recombination of N_2^+. The ground core resonances, in this example, are relatively unimportant compared to those with the excited core. Inclusion of the excited core resonances increases the rate coefficient by about a factor of 4 at room temperature, but the increase is not enough to establish $2^1\Sigma_g^+$ as the dominant dissociative route.

I. Introduction

Dissociative recombination (DR) of ions with electrons is an important process in the ionospheres of planets and moons and in interstellar space.[1] It has been studied in the laboratory in experiments using flowing afterglows and separately in merged beams of ions and electrons,[1,2] and it occurs near the divertors of fusion devices.[3] For the molecular ion, N_2^+, DR is described by

$$N_2^+ + e^- \rightarrow N^* + N^{**} \quad (1)$$

where e^- is an electron and N* and N** are ground or excited states of the N atom. If there are no intermediate states between the reactants and products in eq 1, the process is termed direct DR.[4] In indirect recombination,[5] the electron can be initially captured into a vibrationally excited Rydberg state having the ground ion core, followed by dissociation along the same final state as in eq 1, that is,

$$N_2^+ + e^- \rightarrow N_2^{Ryd} \rightarrow N^* + N^{**} \quad (2)$$
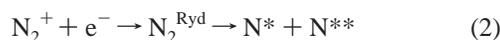
where N_2^{Ryd} denotes a Rydberg state in which the diffuse orbital is attached to the ion ground state. An important process which has received considerably less attention is indirect recombination through excited core Rydberg states, that is,

$$N_2^+ + e^- \rightarrow N_2^{*Ryd} \rightarrow N^* + N^{**} \quad (3)$$
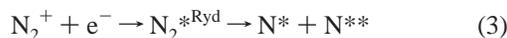
where N_2^{*Ryd} denotes a Rydberg state in which the diffuse orbital is attached to an electronically excited ion. Reactions 2 and 3 appear to be quite similar, but as we will see below, they are driven by very different matrix elements.

Process 3 was first suggested[6] as a mechanism in 1989 and was later included in a theoretical study[7] of the DR of N_2^+ in which only $^3\Pi_u$ dissociative and Rydberg states were treated.

[†] Part of the "Thom H. Dunning, Jr., Festschrift".
* E-mail: slg@sci.org.

In this case, the excited core Rydberg states increase the DR rate by about 10% over the rate obtained without these states. Peaks in the CD^+ DR cross sections derived from storage ring measurements have been assigned to excited core Rydberg states[8] as have peaks in the CH^+ and OH^+ DR cross sections.[9,10] A model calculation[11] has been reported for CD^+. However, several of the necessary couplings were unknown. A later brief report[12] indicated that the inclusion of excited core CH^+ states led to a 2 orders of magnitude increase in the DR cross section at some electron energies. A more detailed paper[13] pointed out that the technique used for the calculation of the various width matrix elements had serious difficulties. In the approach used in this paper, these difficulties are avoided. The two approaches are discussed below.

In this paper, I use the example of the DR of N_2^+ along the $2^1\Sigma_g^+$ dissociative channel to illustrate the important role of excited core Rydberg states in DR. This dissociative channel is one of several states that contributes to the DR of N_2^+. The other states will be reported separately.[14] In the next section, the relevant DR mechanisms are illustrated using the calculated potential curves. In section III, the details of the potential curve calculations are reported. The calculation of the widths is described in section IV, and the multichannel quantum defect theory (MQDT) approach used to calculated the cross sections is reviewed in section V. The results are given in section VI. The conclusions follow in the last section.

II. Dissociative Recombination Mechanisms

The mechanisms for DR that will be considered in this paper are shown in Figure 1 with the calculated potential curves. Shown are the A ion core potential curve with the potential curve for a Rydberg state with a $6p\pi_u$ orbital attached to the A core and the ground state ion curve with the curve for the $6d\sigma_g$ Rydberg state with the ground state core. These particular Rydberg states have been included in Figure 1 only for illustrative purposes. In the calculations described below, all relevant Rydberg states have been included.
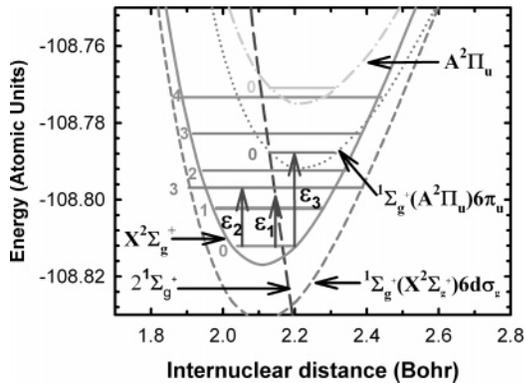
Figure 1. DR Mechanisms. Shown are the $X^2\Sigma_g^+$ ion ground state potential well (solid curve), the $A^2\Pi_u$ excited ion potential well (dot-dashed curve,), the calculated $2^2\Sigma_g^+$ dissociative curve (long dashed curve), the $n = 6$, X core Rydberg state (short dashed curve) and the A core, $n = 6$, Rydberg state (dotted curve). The lowest five vibrational levels of the ion ground state are shown. For clarity, only the $v = 3$ vibrational level is shown for the X core Rydberg well.

The direct[4] DR pathway is shown by the vertical arrow labeled ϵ_1, that is, an electron with this energy can be captured by the $v = 0$ ion into the dissociative $2^1\Sigma_g^+$ state. On the $2^1\Sigma_g^+$ potential, the molecule can separate to atoms or autoionize back to the ion plus an electron. Autoionization can occur as long as the internuclear distance has not increased far beyond the outer turning point of the ion vibrational level. Direct DR is approximately proportional to the square of the overlap between the vibrational wave functions for the ion and dissociative state. A high direct DR rate coefficient is often possible if the repulsive state crosses the ion curve between the turning points of the ion vibrational level, giving a high Franck−Condon factor.

The "traditional" indirect mechanism[5] involves capture into ground core Rydberg states and is shown for an electron at energy ϵ_2 where capture can occur into the $v = 3$ vibrational level of the $n = 6$ Rydberg state. The Rydberg orbital is $6d\sigma_g$ giving a total state symmetry of $^1\Sigma_g^+$. Because the Rydberg and the dissociative state have the same symmetry, these states have an electronic interaction allowing for the predissociation of the Rydberg state. Note that for heuristic purposes, Figure 1 shows the $v = 3$ Rydberg vibrational level to be discrete. However, not only does this state have a width due to predissociation, it is also present in an electron ion continuum and has a width due to auto-ionization. Note that, above the ion, the dissociative state also has a finite width due to auto-ionization.

Capture into an excited core Rydberg state is shown by the arrow labeled ϵ_3. The excited core state in the figure consists of a $6p\pi_u$ orbital bound to the $A^2\Pi_u$ ion core. The total state symmetry is $^1\Sigma_g^+$ allowing for an electronic interaction with the dissociative $2^1\Sigma_g^+$ curve. A significant difference between excited and ground core indirect DR is that all the $v = 0$ levels of the ground core Rydberg states are located below the ion and play no role in DR. On the contrary, there are an infinite number of $v = 0$ Rydberg states with the excited ion core above the $v = 0$ ground ion level. If the minima of the excited core Rydberg potential curves are near the minimum for the ground ion, the largest Franck−Condon factors will be those between the ground ion $v = 0$ level and the $v = 0$ levels in the excited core Rydberg states. Indeed, this is the case for N_2^+. Another significant difference between excited and ground core indirect DR is that electron capture into a ground core Rydberg vibrational level can only occur by Born−Oppenheimer breakdown, because there are no electronic Hamiltonian matrix elements between the ground core Rydberg states and the ground

TABLE 1: Calculated Energies for the $2^1\Sigma_g^+$ Dissociative State

R (a_0)	energy[a] (au)	R (a_0)	energy[a] (au)	R (a_0)	energy[a] (au)
2.0	−0.678559	3.8	−0.941427	6.2	−0.867601
2.07432	−0.746922	3.9	−0.934009	6.3	−0.867397
2.1	−0.767441	4.0	−0.926804	6.4	−0.867220
2.2	−0.834113	4.2	−0.913495	6.5	−0.867064
2.3	−0.883328	4.4	−0.902097	6.6	−0.867171
2.4	−0.919138	4.6	−0.892803	6.7	−0.867120
2.5	−0.944680	4.8	−0.885522	6.8	−0.867073
2.6	−0.962357	5.0	−0.879994	6.9	−0.867031
2.7	−0.973998	5.1	−0.877877	7.0	−0.866992
2.8	−0.980994	5.2	−0.872540	7.1	−0.866955
2.9	−0.984399	5.3	−0.871667	7.2	−0.866921
3.0	−0.985012	5.4	−0.870910	7.3	−0.866890
3.1	−0.983438	5.5	−0.870257	7.4	−0.866860
3.2	−0.980144	5.6	−0.869691	7.5	−0.866833
3.3	−0.975497	5.7	−0.869203	7.6	−0.866806
3.4	−0.969798	5.8	−0.868782	7.7	−0.866782
3.5	−0.963309	5.9	−0.868419	7.8	−0.866759
3.6	−0.956272	6.0	−0.868106	8.0	−0.866739
3.7	−0.948909	6.1	−0.867835		

[a] Add −108 to get the total energy.

ion-electron continuum. The Born−Oppenheimer breakdown interaction (BObi) is accounted for by the variation of the electron quantum defect with the internuclear distance, R, in the MQDT treatment described below. However, for excited core indirect DR, capture can occur by an electronic matrix element, and this interaction can be significantly larger than that due to Born−Oppenheimer breakdown.

The incoming electron can be captured into the ground core Rydberg levels by an additional mechanism in which the dissociative state acts as an intermediate, that is; capture occurs first into the dissociative state followed by transfer to the Rydberg state followed by transfer back to the dissociative state. This is referred to as the indirect second-order mechanism[15] and is included in the calculations described below. In the Born−Oppenheimer breakdown mechanism, capture is most probable for $\Delta v = 1$, but in the electronic mechanism one can have capture into Rydberg states with large Δv. The electronic mechanism for indirect DR is often more important than the Born−Oppenheimer breakdown mechanism.

All these mechanisms are treated simultaneously and are allowed to interfere with each other. The interference plays a major role in determining the shapes of the DR cross sections and the magnitude of the rate coefficients.

III. Potential Curves

The $2^1\Sigma_g^+$ potential curve was calculated in the cc-pVTZ basis of Dunning[16] using the Molecule-Sweden programs.[17] The orbitals were optimized in complete active space self-consistent field (CASSCF)[18] calculations on $2^1\Sigma_g^+$. The active space consisted of 10 electrons in the $2\sigma_g$, $3\sigma_g$, $2\sigma_u$, $3\sigma_u$, $1\pi_g$, and $1\pi_u$ orbitals. The active space wave function had 176 terms and was used as the reference in a singles and doubles configuration interaction (CI) calculation.[19] The calculated energies include the Davidson correction and are given in Table 1. This approach was used for $R \leq 5.0$ a_0. For $R > 5.0$ a_0, the Molpro programs[20] were used. The orbitals[21] were determined in the same manner as for $R \leq 5.0$ a_0, but a contracted CI was used for the final energies.[22] The energies were matched at $R = 5.0$ a_0 leading to a lowering of all the Molpro energies by 0.005 552 au. The calculated potential curve minimum is at $R = 2.9747$ a_0, and the spectroscopic constants are 933.84 cm^{-1}, 2.98 cm^{-1}, 11.02 eV, and 3.22 eV for ω_e, $\omega_e x_e$, T_e, and D_e (the electronic

TABLE 2: Calculated Points for the $X^2\Sigma_g^+$ Potential

R (a_0)	energy^a (au)	R (a_0)	energy^a (au)	R (a_0)	energy^a (au)
1.44	−0.166784	1.68	−0.613683	4.0	−0.546244
1.47	−0.248702	1.69	−0.624126	4.2	−0.535865
1.50	−0.321704	1.7	−0.634095	4.4	−0.527117
1.53	−0.386604	3.1	−0.633198	4.6	−0.519695
1.55	−0.425748	3.2	−0.618216	4.8	−0.513375
1.57	−0.461834	3.3	−0.608006	5.0	−0.507980
1.59	−0.495054	3.4	−0.593380	5.2	−0.503388
1.61	−0.525591	3.5	−0.583133	5.4	−0.499483
1.63	−0.553608	3.6	−0.574065	5.6	−0.496175
1.65	−0.579273	3.7	−0.565983	5.8	−0.493377
1.66	−0.591270	3.8	−0.558733	6.0	−0.491031
1.67	−0.602729	3.9	−0.552190		

^{a} Add −108 to get the total energy.

TABLE 3: Calculated Points for the $A^2\Pi_u$ Potential

R^a (a_0)	energy^b (au)	R^a (a_0)	energy^b (au)	R^a (a_0)	energy^b (au)
1.6	−0.316789	3.2	−0.631371	5.0	−0.510533
1.65	−0.416009	3.3	−0.617383	5.2	−0.506480
1.7	−0.497654	3.4	−0.604602	5.4	−0.503274
1.75	−0.564362	3.5	−0.593010	5.6	−0.500773
1.8	−0.618382	3.6	−0.582556	5.8	−0.498829
1.85	−0.661634	3.7	−0.573165	6.0	−0.497330
1.9	−0.695759	3.8	−0.564745	6.2	−0.496178
2.0	−0.742038	3.9	−0.557201	6.4	−0.495292
2.1	−0.766200	4.0	−0.550435	6.6	−0.494610
2.2	−0.774842	4.1	−0.544358	6.8	−0.494083
2.3	−0.772810	4.2	−0.538887	7.0	−0.493675
2.4	−0.763657	4.3	−0.533954	7.2	−0.493357
2.5	−0.749973	4.4	−0.529499	7.4	−0.493108
2.7	−0.715942	4.5	−0.525474	7.6	−0.492913
2.8	−0.697855	4.6	−0.521836	7.8	−0.492757
2.9	−0.680001	4.7	−0.518551	7.9	−0.492692
3.0	−0.662805	4.8	−0.515590	8.0	−0.492633
3.1	−0.646540	4.9	−0.512925		

^{a} Subtract 0.0083 to get the internuclear distance. ^{b} Add −108 to get the total energy (see text).

dissociation energy), respectively. These are the most accurate constants reported to date for this state. The first calculation[23] on this state was an adjusted minimum basis set approach with a 152 configuration CI wave function. This early calculation predicted R_e, D_e, ω_e, and $\omega_e x_e$ to be 3.08−3.00 a_0, 3.13−4.03 eV, 1135 cm^{-1}, and 6.3 cm^{-1}, respectively, in remarkable agreement with the current calculations. More recent calculations[24] using a smaller scale wave function than that reported here gave 2.99 a_0, 1030 cm^{-1}, 8.8 cm^{-1}, and 10.8 eV for R_e, ω_e, $\omega_e x_e$, and T_e, respectively, in very good agreement with the current results. There are no experimental results for comparison.

For $1.710 \leq R \leq 3.037$ a_0, all potential curve points for the ion ground state are from the RKR potential.[25] For $1.44 \leq R \leq 1.7$ a_0 and for $R \geq 3.1$ a_0, the RKR points are supplemented with additional points calculated with the same approach as for $2^1\Sigma_g^+$ described above except that $X^2\Sigma_g^+$ orbitals are used, and the energies are from the CASSCF calculations. For the small R points, a calculated point at $R = 1.77$ a_0 was shifted to match the RKR point at $R = 1.71$ a_0 where the slopes of the two curves matched. The remaining small R calculated points were equally shifted. The shift for the large R points was determined by shifting the calculated point at $R = 3.037$ to match the RKR point. To use the ion curve with the $2^1\Sigma_g^+$ curve, a calculation similar to that for $2^1\Sigma_g^+$ was done on the neutral N_2 ground state using ground state orbitals. The ion curve is placed at the experimental T_e above the calculated minimum in the ground state potential. With this shift, the minimum of the ion curve is at $E = -108.816\,95$ au. This shift is included in the supplementary points reported in Table 2.

The $A^2\Pi_u$ ion was determined in a manner similar to that of the $2^1\Sigma_g^+$ state except that the Dunning[16] cc-pVQZ set was used.[20] For the spectroscopic constants, there is excellent agreement between theory and experiment. The calculated (experimental)[25] values for ω_e, $\omega_e x_e$, and R_e are 1898 (1904 cm^{-1}), 14.9 (15.0 cm^{-1}), and 2.2261 (2.2178 a_0). In the DR calculations, the A state was shifted by 0.0083 a_0 to the experimental R_e and placed at the experimental T_e above the X ion state. The shifted A curve is in Table 3.

IV. Widths

The technique for the calculation of the electron capture widths has been described previously.[15,26] Here, I will focus upon issues relevant to DR by $2^1\Sigma_g^+$. The probability of electron capture and autoionization is governed by an electronic width, $\Gamma(R)$. The direct DR cross section is approximately directly proportional to $\Gamma(R)$, which is given by

$$\Gamma_{ion,d}^{\epsilon}(R) = 2\pi\langle\{\Phi_{ion}(x, R)\,\varphi_\epsilon(x, R)\}|H|\Phi_d(x, R)\rangle^2 \quad (4)$$

where H is the electronic Hamiltonian, R is the internuclear distance, the integration is over the electronic coordinates represented by x, and the electronic wave functions from left to right are for the ion core, the free electron, and the dissociative neutral state. ϵ is the free electron energy. The antisymmetrized product of the ion core and free electron wave functions is denoted by {}. CI wave functions are used on both sides of the matrix element in eq 4.

Let us first look at the calculation of Γ for the capture of an electron by N_2^+, $X^2\Sigma_g^+$, into $2^1\Sigma_g^+$. To take advantage of bound state techniques, the continuum orbital, φ_ϵ, is replaced by a high Rydberg orbital. The coordinate space sampled by the integrand in eq 4 is near the nuclei because of the tight valence orbitals. In this region, the continuum (for $\epsilon = 0$) and high Rydberg orbitals show a similar amplitude variation and the $\epsilon = 0$ orbitals can be replaced by a high Rydberg orbital multiplied by a density of states, ρ, where

$$\rho = 1/(E(n^* - 1/2) - E(n^* + 1/2)) \approx n^{*3}$$

E is the energy of a Rydberg state, and n^* is the effective principal quantum number. ρ is needed to convert the normalization of the Rydberg orbital to that for a continuum orbital containing a free electron. For the matrix element in eq 4 to be nonzero for ground ion capture into $2^1\Sigma_g^+$, the high Rydberg orbital must be of σ symmetry. These orbitals are represented by a large diffuse primitive Gaussian basis centered at the midpoint of the internuclear axis. The orbital exponents are determined from the formula of Kaufmann et al.[27] Using 18 primitive Gaussians, it is possible to represent Rydberg states up to $n = 10$, where n is the principal quantum number. For the $\ell = 2$, $nd\sigma$ Rydberg orbitals, these 18 Gaussian exponents range from 0.060 54 to 0.000 124 6. Note that the case $ns\sigma$ will be reported separately in a study of the total DR rate coefficient.[14] In this paper, the discussion is restricted to the $\ell = 2$, $nd\sigma$, orbitals to illustrate the important role of excited core Rydberg states.

The valence orbitals used on both sides of eq 4 are expanded in a cc-pVDZ basis[16] with the orbital coefficients determined in a CASSCF calculation on the ion ground state having nine active electrons. The Rydberg orbital coefficients are determined in Improved Virtual Orbital[28] calculations which use the valence orbitals from the CASSCF on the ion. The Rydberg orbitals are determined in the field of the ion using a Hamiltonian that

TABLE 4: Electronic Widths for $2^1\Sigma_g^+$ in the $X^2\Sigma_g^+$ Continuum and Quantum Defects

R^a (a_0)	Γ (eV)	μ	R^a (a_0)	Γ (eV)	μ
1.9	0.00925	0.0985	2.5	0.0137	0.0830
2.0	0.0111	0.1034	2.6	0.0128	0.0771
2.0743		0.1063	2.7	0.00642	0.0650
2.1	0.0126		2.8	0.00685	0.0493
2.2	0.0131	0.1096	2.9	0.00101	0.0335
2.3	0.0140	0.1007	3.0	0.00015	0.0147
2.4	0.0138	0.0998			

^{a} Subtract 0.0398 to get the internuclear distance.

is appropriate for the overall $^1\Sigma_g^+$ symmetry. The optimized Rydberg orbital is coupled to the CASSCF ion wave function to form the wave function on the left side of eq 4. Additional configurations are included which have virtual orbitals (with the same symmetry as the Rydberg orbital) coupled to the ion.

From the energy difference, E, between the multiconfiguration ion and Rydberg states, the quantum defect, μ, is determined from the expression $\mu = n - 1/(2E)^{1/2}$, where n is the principal quantum number. The quantum defect, which energetically characterizes the Rydberg series relative to the ion, is an important input parameter to the MQDT approach described below. The quantum defects in Table 4 are based upon the assignment of $n = 3$ to the lowest energy state dominated by diffuse d character. A previous study[29] has assigned $n = 4$ to the lowest dσ Rydberg state leading to an increase by unity in the quantum defects compared to those reported here. The increase by unity affects only the labeling of the states and has no physical effect. The quantum defect calculated here is 0.1063 at $R = 2.0345$ a_0 and compares to 1.0325[29] at $R = 2.1$ a_0 (or 0.0325 for comparison) obtained numerically in the field of a frozen core Hartree−Fock description of the ion ground state. The result reported here is more accurate than the prior result because of a multiconfiguration description of the ion and Rydberg states and the avoidance of a frozen core approximation.

The wave function for the dissociative state (in the width calculation only) is a full CI within the space of the valence orbitals. In addition, the multiconfiguration wave function for the ion plus a Rydberg electron is allowed to mix in higher nonphysical correlating roots from the space of configurations describing the dissociative state. This procedure allows an important additional correlation to mix into the electron-ion states.[6,30]

The most important Rydberg configuration in the width matrix element near the ion R_e is

$$... 2\sigma_g^2 \, 2\sigma_u^2 \, 3\sigma_g \, 1\pi_{ux}^2 \, 1\pi_{uy}^2 \, nd\sigma \qquad (5)$$

where ... denotes the core orbitals, $1\sigma_g^2 \, 1\sigma_u^2$. The most important configuration in the $2^1\Sigma_g^+$ state is

$$... 2\sigma_g^2 \, 2\sigma_u^2 \, 3\sigma_g^2 \, 1\pi_{ux} \, 1\pi_{uy} \, 1\pi_{gx} \, 1\pi_{gy} \qquad (6)$$

The configuration in eq 6 differs from that in eq 5 by a triple excitation, and the width matrix element between these two configurations is zero. If there is no contribution to the matrix element in eq 4 by the major configurations, the total matrix element is often quite small. The calculated matrix elements as a function of R are given in Table 4. The matrix elements are from the $n = 8$, 9, and 10 Rydberg orbitals. Indeed, the matrix elements are quite small as expected. Also shown are the quantum defects. The variation of the defect with R is a measure of the amplitude of the Born−Oppenheimer breakdown interac-

TABLE 5: Electronic Widths for $2^1\Sigma_g^+$ in the $A^2\Pi_u$ Continuum and Quantum Defects

R (a_0)	Γ (eV)	μ	R (a_0)	Γ (eV)	μ
1.8	0.122	0.6201	2.4	0.233	0.5365
1.9	0.136	0.6106	2.5	0.264	0.5266
2.0	0.152	0.5870	2.6	0.308	0.5007
2.1	0.168	0.5724	2.7	0.319	0.4864
2.2	0.187	0.5593	2.9	0.416	0.4959
2.3	0.208	0.5473	3.0	0.482	0.4904

^{a} Subtract 0.0469 to get the internuclear distance.

TABLE 6: Electronic Widths Connecting the Excited and Ground Core States

R^a (a_0)	Γ (eV)	R^a (a_0)	Γ (eV)	R^a (a_0)	Γ (eV)	R^a (a_0)	Γ (eV)
1.8	0.403	2.2	0.406	2.5	0.376	2.8	0.325
1.9	0.409	2.3	0.399	2.6	0.361	2.9	0.305
2.0	0.411	2.4	0.389	2.7	0.344	3.0	0.285
2.1	0.410						

^{a} Subtract 0.0433 to get the internuclear distance.

tion (BObi) between the continuum electron and the nuclei. The calculated defects vary only slowly with R. Because the BObi is small, the capture of the continuum electron into the ground core Rydberg levels is not expected to be important. Because of the small width matrix element, the direct cross section for DR is also expected to be small.

Another width matrix element needed for these calculations involves the excited core Rydberg states on the left of eq 4 and the $2^1\Sigma_g^+$ state on the right. These matrix elements are needed for the description of the predissociation of the excited core Rydberg states formed in the initial electron capture. The most important configuration of the excited core Rydberg states is

$$... 2\sigma_g^2 \, 2\sigma_u^2 \, 3\sigma_g^2 \, 1\pi_{ux}^2 \, 1\pi_{uy} \, np\pi_{uy} \qquad (7)$$

and the equivalent configuration with x and y interchanged. Note that in order to have $^1\Sigma_g^+$ symmetry, the Rydberg orbital is π_{uy}. This configuration differs by a double excitation from that in eq 6, and the most important terms in the two wave functions will contribute to the total matrix element in eq 4. Therefore, widths that are greater than those for the ground ion core are expected for this case. This expectation is borne out by the calculated widths shown in Table 5.

The last type of width needed for these calculations governs the capture of the continuum electron into the excited core Rydberg states. As already discussed above, this process is driven by an electronic matrix element in which an excited core Rydberg state replaces the dissociative state on the right side of eq 4 and the ground state ion continuum or Rydberg state remains on the left side. Configurations 5 and 7 differ by a double excitation, and the widths are large as shown in Table 6. Note that the widths in Table 6 are for a free electron on either side of eq 4. Two densities of states are needed in this case, one for each Rydberg state. The matrix elements were calculated using the $n = 10$ Rydberg state for the ground ion core and the $n = 4$ Rydberg state for the excited core state. The latter state is important in the threshold region for DR as is shown below.

In the calculations[13] referred to in the Introduction, the authors determined the width for the interaction of the dissociative state with the Rydberg states by adding the main configuration of the dissociative state to a diabatic representation of the Rydberg states. The width is obtained from the energy shift of the Rydberg state. While this method should work in principle, it suffers from inaccuracy because of the representation of the

dissociative state by only a single configuration. This approach has also been used for calculating the widths describing the interaction of the ground and excited core Rydberg states. However, as pointed out by the authors, neighboring Rydberg states of one series can cause opposite shifts in a Rydberg state of another series, making it difficult to extract an accurate width. These problems do not occur in the approach used in this paper because the width matrix element is calculated directly from a multiconfiguration wave function for each state.

V. Multichannel Quantum Defect Theory Approach

The MQDT approach to calculating the DR cross sections and rate coefficients has been discussed previously.[15,31,32] Here, I give only a brief description of the highlights that are relevant to the N_2^+ calculations. The general approach described previously[31] is followed here with revisions for the second-order $\mathbf{K}$ matrix[15] and the excited core states. The $\mathbf{S}$ matrix is calculated using an approach attributed to Seaton.[33,34] Although a relatively simple expression[31,35] can be used to calculate the direct DR cross section, no such expression has been derived for the full cross section that includes both direct and indirect DR. The MQDT approach includes both the direct and indirect processes on an equal footing and accounts for the interference between both. This method is based upon the Lippmann–Schwinger equation,

$$\mathbf{K} = V + VG\mathbf{K} \tag{8}$$

where G is a standing wave Green operator and $\mathbf{K}$ is the reaction matrix that includes all the electronic interactions. $\mathbf{V}$ is the interaction matrix,

$$\mathbf{V}_{vd} = \langle \chi_v(R) | (\Gamma^\epsilon_{ion,d}(R)/2\pi)^{1/2} | \chi_d(R) \rangle \tag{9}$$

where χ_v and χ_d are vibrational wave functions for the ion and the dissociative state and $\Gamma^\epsilon_{ion,d}$ is from eq 4. Because $\mathbf{K}$ appears on both sides of the Lippmann–Schwinger equation, $\mathbf{K}$ is determined by a perturbative approach. In the calculations described in this paper, $\mathbf{K}$ is calculated to second order in the interaction matrix elements, $\mathbf{V}$, that is,

$$\mathbf{K} \approx \mathbf{V} + \mathbf{V}G\mathbf{V} \tag{10}$$

With the inclusion of the second term on the right of eq 10, the method describes interactions in which $\mathbf{V}$ acts twice. An example is capture of a free electron into the dissociative state followed by transfer from the dissociative state to the Rydberg vibrational level. This mechanism competes with the BObd mechanism for capture into the Rydberg vibrational levels. The BObd mechanism is also included in the calculations. The second-order term also connects excited vibrational levels to each other via the dissociative state, that is, levels other than the initial ion level. For more information on the calculation of the $\mathbf{K}$ matrix, the reader is referred to ref 15.

From the $\mathbf{K}$ matrix, eigenchannels are generated in which the total wave function is expressed in terms of the eigenvectors and eigenvalues of the $\mathbf{K}$ matrix. A frame transformation is then used to define R independent coefficients from which the scattering matrix and the cross section can be calculated.

VI. Cross Sections and Rate Coefficients

The nuclear wave functions were determined on a grid of 7000 points for $R = 1.0-8.0$ a_0. For the X and A states, 18 vibrational levels for each ion were included in the calculations. The calculated direct cross section is shown in Figure 2 with
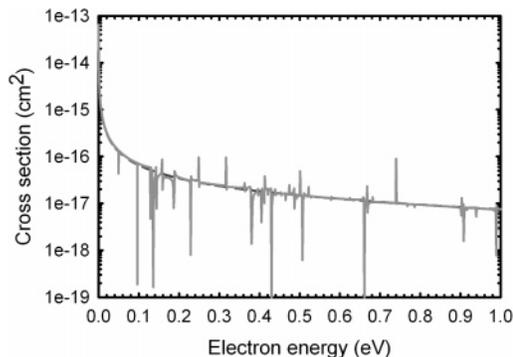
Figure 2. $v = 0$ DR cross section without excited core Rydberg states (solid curve). The direct cross section (dashed curve).
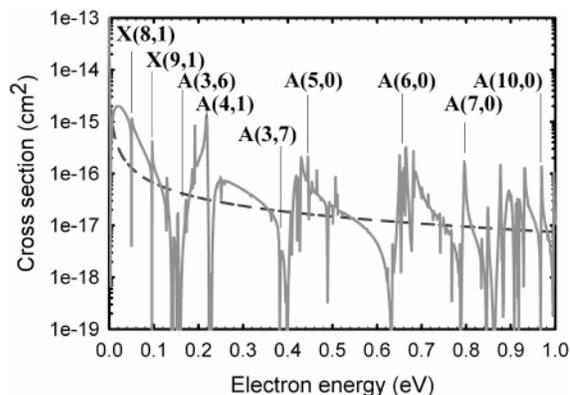
Figure 3. $v = 0$ DR cross section including the excited core Rydberg states (solid curve). The direct cross section (dashed curve). Several resonances are labeled with the core state followed by (n, v) where n is the principal quantum number and v is the vibrational level.

the cross section that includes the ground core but not the excited core Rydberg levels. The smoothly varying direct cross section (without resonances) shown with a dashed line is nearly coincident with the full cross section. Structure in the DR cross sections is due to the interference between dissociation arising from direct capture into the dissociative state and that due to indirect capture into Rydberg states followed by predissociation. The narrow structures in the full cross section are due to the vibrationally excited Rydberg states. However, the small electron capture and predissociation widths cause the ground ion Rydberg levels to play only a minor role in DR.

Figure 3 has the DR cross section including both ground and excited core Rydberg levels. There is a striking difference between the cross sections shown in Figure 2 and those shown in Figure 3. The widths for entering the excited core Rydberg levels from the ground core electron-ion continuum and the widths for predissociation of these levels are much higher than the same widths for the ground ion Rydberg levels. The result is that the resonance structure is due almost entirely to the excited core levels. The resonance structure is labeled with the associated ion core and, in parentheses, the principal quantum number and vibrational level. The $n = 8, 9$ $v = 1$ levels with the X core, apparent also in Figure 2, are now superimposed upon a broad resonance structure between 0.0 and 0.1 eV. In this important region for room temperature rate coefficients, the cross section is nearly 1 order of magnitude higher than the direct cross section and the cross section obtained without excited core states.

To understand the source of the resonance structure, the cross section including only the $v = 0$ excited ion core resonances is shown in Figure 4 with the direct cross section. This series of resonances has its limit at 1.12 eV above the ground ion $v = 0$
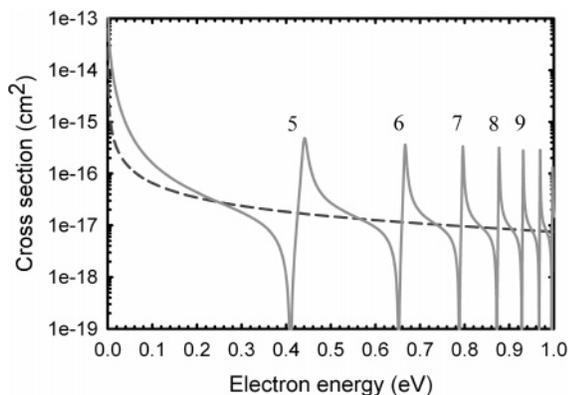
Figure 4. Direct DR cross section (dashed curve) and the DR cross section including only the excited core $v = 0$ resonances.
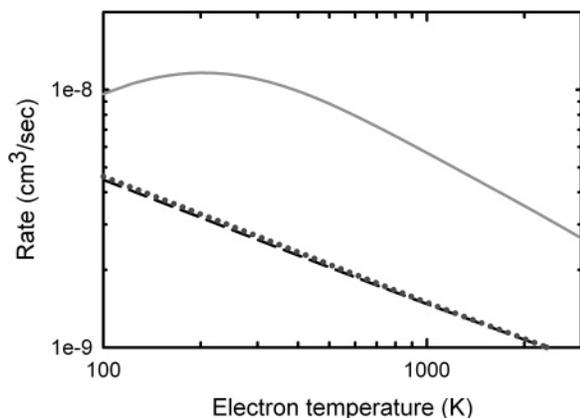
Figure 5. Full DR rate constant (solid curve). The direct DR (dotted curve) and the rate constant calculated with only the ground core Rydberg states (dashed curve) are nearly indistinguishable.

level at the $v = 0$ level of the A state. The resonances become narrower as $1/(n - \mu)^3$ because the width is given by

$$\Gamma_n = [2\pi/(n - \mu)^3]\mathbf{V}_{vd}^2 \tag{11}$$

where $\mathbf{V}_{vd}$ is from eq 9 with $\epsilon = 0$. Comparing Figures 3 and 4, it can be seen that the increase of the cross section above the direct cross section below 0.1 eV is due to the high-energy wing of the $n = 4$ resonance. The center of the $n = 4$ resonance lies below the threshold. The assignment of this feature to the $v = 0$ level is confirmed by the analysis of additional cross sections including resonances with higher v values. That the $v = 0$ levels are so prominent is not a surprise considering that the $v = 0$ level of the A state has the largest Franck−Condon factor with the $v = 0$ ground ion wave function, and the lowest n states have the largest widths in accord with eq 11. Further comparison of Figures 3 and 4 shows that the $n \geq 4$, $v = 0$ pπ excited core resonances play a prominent role in determining the resonance structure. The complex resonance structure seen in the cross section is due not only to interference between the DR mechanisms discussed above but also to interference between members of the Rydberg series having the A state as a core.

Figure 5 shows the $v = 0$ rate coefficients for direct DR, DR with both ion cores, and DR with only the ground ion core. As expected from the above discussion, the direct DR and ground core only rate coefficients are nearly identical. At 300 K, the two core rate coefficient, 1.1×10^{-8} cm^3/s, is about 4 times higher than the one core rate coefficient. This difference is due mostly to the $v = 0$ excited core resonances.

There are no prior theoretical descriptions of the DR rate constant or cross section along $2^1\Sigma_g^+$. Storage ring,[36,37] microwave afterglow,[38−41] and merged beam single pass[42] experiments on the DR of N_2^+ have been reported. The $2^1\Sigma_g^+$ dissociative route reported here is one of several dissociative routes that contribute to the DR of N_2^+ from $v = 0$. The other routes are of $^3\Pi_u$, $^1\Pi_u$, and $^1\Sigma_u^+$ symmetries[43] and will be reported separately. The $2^1\Sigma_g^+$ contribution[14] is about 5% of the total DR rate and contributes about 0.1 to the total N(^{2}D) quantum yield because it dissociates to two N(^{2}D) atoms. Even though the excited core states have substantially increased the DR rate along this route, the increase is not enough to make $2^1\Sigma_g^+$ a dominant route.

$2^1\Sigma_g^+$ has a unique product angular distribution which would allow the $2^1\Sigma_g^+$ contribution to be detected experimentally by measuring the projected distance distributions of the products. These measurements have already been made for several molecular ions[1,9] including N_2^+.[36,37] In the case of $2^1\Sigma_g^+$, rules[44] for predicting the angular distribution of the products indicate that this is the only route among the above symmetries that leads to the superposition of an isotropic (from the sσ wave not treated in this paper) and a $(3 \cos^2 \theta - 1)^2$ (from the dσ wave) product distribution at nonzero electron energies where θ is the angle between the internuclear axis and the electron beam. However, the prior storage ring measurements[36,37] of the product distributions were only done at 0 eV where all routes yield isotropic distributions. Therefore, there are no experimental data for comparison to the current results for $2^1\Sigma_g^+$. Future storage ring measurements at nonzero electron energies with measurement of the projected distance product distributions would be a valuable contribution.

VII. Conclusions

I have shown that excited core resonances can play an important role in DR cross sections and rate coefficients. However, the excited core resonances may not be sufficient to convert a DR route into the dominant pathway for DR. The role of excited core states in other molecules can be predicted from a simple query into the main configuration structure of the dissociative and Rydberg states. If, as discussed in this paper, the main ground core Rydberg configuration differs from the main dissociative configuration by a triple electronic excitation or more, the electronic widths will be small. If the main excited core Rydberg configuration differs from the main dissociative configuration by a double excitation, the electronic widths are likely to be of a magnitude that cannot be neglected. If both ground and excited core Rydberg states differ by a double excitation from the main dissociative configuration both sets of Rydberg states are likely to be important, and a complex resonance structure will result from the interference between the series. These considerations assume that the ion is energetically situated such that the excited core states can fall near the ground ion $v = 0$ level.

But will the presence of excited core states, in the DR of other ions, increase or decrease the cross section? This question cannot be answered without detailed calculations such as those presented here. The effect upon the cross section in a specified energy range is dependent upon the location of the resonances and the nature of the interference with the background direct DR. For example, the $v = 0$ resonances shown in Figure 4 show constructive interference with the direct DR background at energies above the resonance center and destructive interference below the resonance center. If this interference pattern were

reversed, the cross sections below 0.1 eV would be less than the direct cross section, and the rate constant at room temperature would be below the direct rate.

References and Notes

(1) (a) *Sixth International Conference on Dissociative Recombination: Theory, Experiment and Applications*; Wolf, A., Lammich, L., Schmelcher, P., Eds.; Journal of Physics Conference Series; Institute of Physics: London, 2005; Vol. 4. (b) *Dissociative Recombination of Molecular Ions with Electrons*; Guberman, S. L., Ed.; Kluwer Academic/Plenum: New York, 2003.

(2) Florescu-Mitchell, A. I.; Mitchell, J. B. A. *Phys. Rep.* **2006**, *430*, 277.

(3) Janev, R. K. Role of Dissociative Recombination and Related Molecular Processes in Fusion Edge Plasmas. In *Dissociative Recombination: Theory, Experiment and Applications*; Larssen, M., Mitchell, J. B. A., Schneider, I. F., Eds.; World Scientific: Singapore, 2000; p 40.

(4) Bates, D. R. *Phys. Rev.* **1950**, *78*, 492.

(5) Bardsley, J. N. *J. Phys. B* **1968**, *1*, 365.

(6) Guberman, S. L. Ab initio studies of Dissociative Recombination. In *Dissociative Recombination: Theory, Experiment and Applications*; Mitchell, J. B. A., Guberman, S. L., Eds.; World Scientific: Singapore, 1989; p 45.

(7) Guberman, S. L. New Mechanisms for Dissociative Recombination. In *The Physics of Electronic and Atomic Collisions, Invited Papers for the XIX International Conference*; Dube, L. J., Mitchell, J. B. A., McConkey, J. W., Brion, C. E., Eds.; American Institute of Physics Press: New York, 1995; p 307.

(8) Forck, P.; et al. *Phys. Rev. Lett.* **1994**, *72*, 2002.

(9) Amitay, Z.; et al. *Phys. Rev. A* **1996**, *54*, 4032.

(10) Amitay, Z.; et al. *Phys. Rev.* **1996**, *53*, R644.

(11) Carata, L.; Schneider, I. F.; Suzor-Weiner, A. *Phil. Trans. R. Soc. London, Ser. A* **1997**, *355*, 1677.

(12) Carata, L.; Orel, A. E.; Schneider, I. F.; Suzor-Weiner, A. Core Excited Resonances in the Dissociative Recombination of CH^+ and CD^+. In *Dissociative Recombination: Theory, Experiment and Applications*; Larssen, M., Mitchell, J. B. A., Schneider, I. F., Eds.; World Scientific: Singapore, 2000; p 291.

(13) Carata, L.; Orel, A. E.; Raoult, M.; Schneider, I. F.; Suzor-Weiner, A. *Phys. Rev. A* **2000**, *62*, 052711.

(14) Guberman, S. L. To be submitted for publication.

(15) Guberman, S. L.; Suzor-Weiner, A. *J. Chem. Phys.* **1991**, *95*, 2602.

(16) Dunning, T. H., Jr. *J. Chem. Phys.* **1989**, *90*, 1007.

(17) Siegbahn, P. E. M.; Bauschlicher, C. W.; Roos, B.; Taylor, P. R.; Almlöf, J. *Molecule-Sweden.*

(18) Siegbahn, P.; Heilberg, A.; Roos, B.; Levy, B. *Phys. Scr.* **1980**, *21*, 323.

(19) Siegbahn, P. E. M. *J. Chem. Phys.* **1980**, *72*, 1647.

(20) Werner, H.-J.; Knowles, P. J. *MOLPRO*: a package of ab initio programs (with contributions from Almlöf, J.; Amos, R. D.; Deegan, M. J. O.; Elbert, S. T.; Hampel, C.; Meyer, W.; Peterson, K.; Pitzer, R.; Stone, A. J.; Taylor, P. R.; Lindh, R.).

(21) Werner, H.-J.; Knowles, P. J. *J. Chem. Phys.* **1985**, *82*, 5053. Knowles, P. J.; Werner, H.-J. *Chem. Phys. Lett.* **1985**, *115*, 259.

(22) Werner, H.-J.; Knowles, P. J. *J. Chem. Phys.* **1988**, *89*, 5803. Knowles, P. J.; Werner, H.-J. *Chem. Phys. Lett.* **1988**, *145*, 514.

(23) Michels, H. H. *J. Chem. Phys.* **1970**, *53*, 841.

(24) Ermler, W. C.; Clark, J. P.; Mulliken, R. S. *J. Chem. Phys.* **1986**, *86*, 370.

(25) Lofthus, A.; Krupenie, P. H. *J. Phys. Chem. Ref. Data* **1977**, *6*, 113.

(26) Guberman, S. L. *J. Chem. Phys.* **1995**, *102*, 1699.

(27) Kaufmann, K.; Baumeister, W.; Jungen, M. *J. Phys. B* **1989**, *22*, 2223.

(28) Hunt, W. J.; Goddard, W. A., III. *Chem. Phys. Lett.* **1969**, *3*, 414.

(29) Chung, S.; Lin, Chun, C.; Lee, E. T. P. *J. Chem. Phys.* **1985**, *82*, 342.

(30) Hazi, A. U. Molecular Resonance Phenomena. In *Electron-Atom and Electron-Molecule Collisions*; Hinze, J., Ed.; Plenum: New York, 1983; p 103.

(31) Giusti, A. *J. Phys. B* **1980**, *13*, 3867.

(32) Lee, C. M. *Phys. Rev. A* **1977**, *16*, 109.

(33) Nakashima, K.; Takagi, H.; Nakamura, H. *J. Chem. Phys.* **1987**, *86*, 726.

(34) Seaton, M. J. *Rep. Prog. Phys.* **1983**, *46*, 167.

(35) Flannery, M. R. *Adv. At., Mol., Opt. Phys.* **1994**, *32*, 117.

(36) Kella, D.; Johnson, P. J.; Pedersen, H. B.; Vejby-Christensen, L.; Andersen, L. H. *Phys. Rev. Lett.* **1996**, *77*, 2432.

(37) Petersen, J. R.; Le Padellec, A.; Danared, H.; Dunn, G. H.; Larsson, M.; Larson, Å.; Peverall, R.; Strömholm, C.; Rosén, S.; af Ugglas, M.; van der Zande, W. J. *J. Chem. Phys.* **1998**, *108*, 1978.

(38) Mehr, F. J.; Biondi, M. A. *Phys. Rev.* **1969**, *181*, 264.

(39) Zipf, E. C. *Geophys. Res. Lett.* **1980**, *7*, 645.

(40) Geoghegan, M.; Adams, N. G.; Smith, D. *J. Phys. B* **1991**, *24*, 2589.

(41) Canosa, A.; Gomet, J. C.; Rowe, B. R.; Queffelec, J. L. *J. Chem. Phys.* **1991**, *94*, 7159.

(42) Mul, P. M.; McGowan, J. Wm. *J. Phys. B* **1979**, *12*, 1591.

(43) Guberman, S. L. The Dissociative Recombination of N_2^+. In *Dissociative Recombination of Molecular Ions with Electrons*; Guberman, S. L., Ed.; Kluwer Academic/Plenum: New York, 2003; p 187.

(44) Guberman, S. L. *J. Chem. Phys.* **2004**, *120*, 9509.